

A 39.5-dB SNR, 300-Hz Frame-Rate, 56 × 70-Channel Read-Out IC for Electromagnetic Resonance Touch Panels

SangYun Kim, SungHun Cho, *Student Member, IEEE*, YoungGun Pu , Sang-Sun Yoo , *Member, IEEE*, Minjae Lee, Keum Cheol Hwang , *Senior Member, IEEE*, Youngoo Yang, and Kang-Yoon Lee, *Senior Member, IEEE*

Abstract—In this paper, a pen detection analog system for an electromagnetic resonance (EMR) touch panel is presented. An adaptive charge pump is proposed in the transmitter to drive a high current to the EMR panel and achieve a high signal-to-noise ratio (SNR) in the receiver. To compensate for the mismatches between the channels due to fabrication variations of the EMR panels and process variations of the analog front-ends (AFEs), a transmitter driver with an adaptive controller is proposed, and an AFE calibration is implemented in the transmitter and the receiver, respectively. Also, a 9-bit, 2-MS/s time-interleaved flash successive-approximation-register (SAR) analog-to-digital converter (ADC) with 3-bit flash and 6-bit SAR ADCs is proposed to increase the frame rate with small area and power consumption. External noises, such as display and charger noises, can be rejected by the differential processing, analog low-pass filter, and digital filters in the digital signal processor (DSP). This read-out integrated circuit is implemented in a 0.18- μm Bipolar-CMOS-DMOS (BCD), and the die area is 40 mm² including DSP and ADCs. The power consumptions are 110 and 45 mW in the transmitter and receiver modes, respectively. The SNR is about 39.5 dB and the frame rate is about 300 Hz in the 56 × 70 touch panel.

Index Terms—Analog front-end (AFE), analog-to-digital converter (ADC), electromagnetic resonance (EMR) touch panel, low-pass filter (LPF), pen touch system, variable-gain amplifier (VGA).

Manuscript received March 27, 2017; revised June 20, 2017 and September 1, 2017; accepted October 20, 2017. Date of publication November 13, 2017; date of current version February 13, 2018. This work was supported by Basic Science Research Program through the National Research Foundation of Korea (NRF) funded by the Ministry of Science, ICT and Future Planning under Grant NRF-2017R1A2B3008718. (Corresponding author: Kang-Yoon Lee.)

S. Kim, S. Cho, Y. Pu, K. C. Hwang, Y. Yang, and K.-Y. Lee are with the College of Information and Communication Engineering, Sungkyunkwan University, Suwon 440-746, South Korea (e-mail: ksy0501@skku.edu; csh1107@skku.edu; hara1015@naver.com; khwang@skku.edu; yang09@skku.edu; klee@skku.edu).

S.-S. Yoo is with the Department of Smart Automobile, Pusan National University, Pusan 462-743, South Korea (e-mail: rapter@kaist.ac.kr).

M. Lee is with the School of Information and Communications, Gwangju Institute of Science and Technology, Gwangju 61005, South Korea (e-mail: minjae@gist.ac.kr).

Color versions of one or more of the figures in this paper are available online at <http://ieeexplore.ieee.org>.

Digital Object Identifier 10.1109/TIE.2017.2772145

I. INTRODUCTION

RECENTLY, the demand for touch screen panels has increased for various applications such as smartphones, tablets and touch monitors [1]–[3]. As touch technology develops further, touching a screen with a pen or fingers has developed actively in the electronics industry [4], [5]. Among the many objects possible, the use of a pen is most prominent. A pen is an input device for users to write on the touch screen surface of an electronic device such as a mobile phone, tablet, or laptop computer [6]–[8]. In general, there are many types of touch panels such as resistive, capacitive, surface acoustic wave, and infrared [9]. In addition, the manufacturing of the touch sensor is divided into two kinds of methods. First, in-cell touch sensors are physically inside the liquid-crystal display (LCD) cell. In-cell touch technology is applied to touch sensors that are integrated into plasma-display panels, electrophoretic (electronic paper) displays, and organic light-emitting diodes. Second, out-cell touch sensors require an additional piece of glass. Out-cell touch is used for the integration of an LCD-module manufacturer [10]. The out-cell touch structure is used in the proposed architecture.

The electromagnetic resonance (EMR) touch panel is composed of a thin sheet, in which many overlapping loop coils are placed in a matrix in the x- and y-axis directions. It has more advantages than other touch panels. The increasing cost of the touch panel is significantly reduced as the size of the sensor increases. The quality and brightness of the display screen are not reduced and the panel is not touched directly because the touch panel is located behind the display screen. Therefore, the durability of the touch panel is extremely high. In addition, it is possible to detect even small characters written using the pen because the EMR touch panel has high precision and high resolution [11].

Fig. 1 shows an EMR touch system between a pen and a touch panel. The proposed design operates with the EMR touch pen. After transmitting the signal to the pen, the touch panel receives the electromagnetic field to be activated in the pen. If the pen is located near the panel, the coil of the pen is resonated and the resonance signal of the pen is delivered to the touch panel. This system identifies the location by detecting the resonant magnitude of the pen signal.

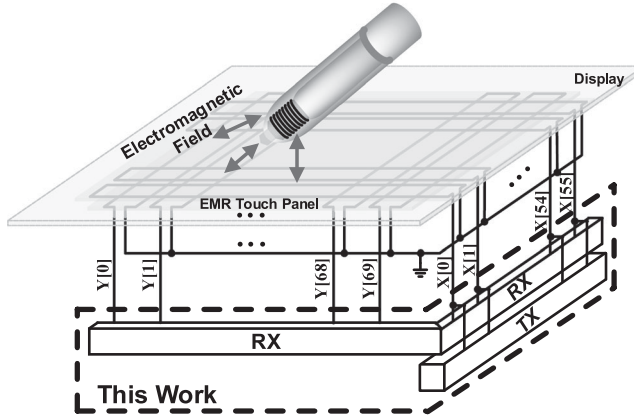


Fig. 1. EMR touch system.

The conventional architectures for a touch panel are composed of charge amplifiers, integrators, an analog to digital converter (ADC) and a digital signal processor (DSP). The ADC and DSP blocks are not included in the chip [12]–[17]. In addition, to scan many channels quickly on a touch panel by the multiplexer (MUX), the architecture of a multipath analog frontend (AFE) is implemented [12]–[15]. Typically, the transmitter (TX) for the touch panel applies the same or slightly higher voltage than the receiver's (RX) supply voltage [12], [17].

In this paper, in order to effectively detect a pen on the panel, an AFE for the EMR touch panel is presented. To achieve the high signal-to-noise ratio (SNR) and guarantee the uniformity of the SNR at each channel of the panel, an AFE with an adaptive charge pump, calibration, and a low-pass filter (LPF) with filter tuning are proposed. Thanks to the adaptive charge pump, the output resonance voltage of the pen is increased and the SNR is improved. By adopting the adaptive charge pump, it can compensate for the different voltage levels due to the parasitic resistance of the inductive coil in each channel. In order to reduce the mismatch of the AFE when the touch signal is processed, the AFE calibration and the LPF with filter tuning are implemented. Two variable-gain amplifiers (VGAs) with wide gain range and fine resolution are designed to amplify the small signal from the panel and improve the accuracy of the seven paths for the SNR. The LPF with filter tuning is designed to decrease the sensitivity to the process variations [18]. Also, a 9-bit time-interleaved flash SAR with 3-bit flash and 6-bit SAR ADC is proposed to increase the frame rate with small area.

II. SYSTEM ARCHITECTURE

Fig. 2(a) shows the model of the EMR pen on the touch panel. C_{pen} and L_{pen} are the capacitor and inductive coil in the pen, respectively. L_{panel} represents the inductive coil in the panel. By coupling L_{panel} and L_{pen} , the position of the pen can be detected. Fig. 2(b) illustrates the circuit model of an EMR pen and the panel. R_{panel} and C_{panel} represent the resistance of the inductive coil and the parasitic capacitance between the inductive coils, respectively.

In the TX mode of the panel, the TX driver transmits the signal to L_{panel} , which forms the magnetic field and generates

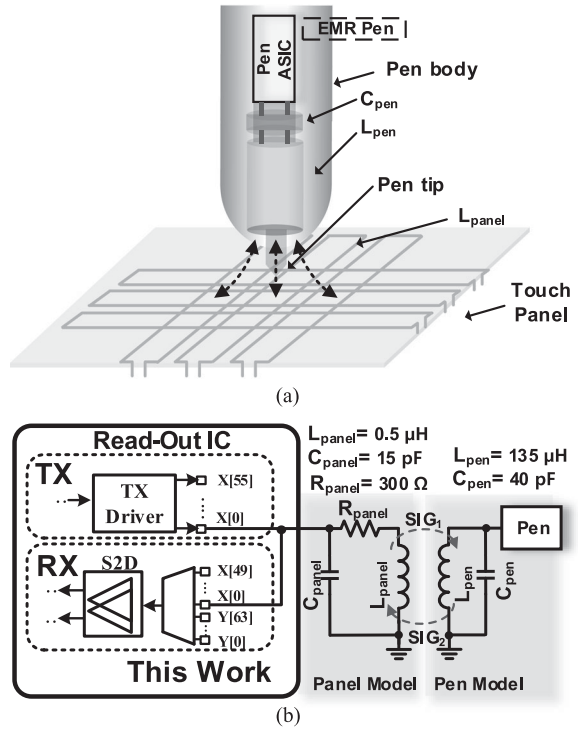


Fig. 2. (a) Model of an EMR pen on the touch panel. (b) Circuit model of an EMR pen and the panel.

the signal, SIG_1 , in the TX mode of the panel. If the pen is located on the panel, the magnetic field (SIG_1) of L_{panel} is coupled with L_{pen} . L_{pen} and C_{pen} can be resonated using the delivered signal from the panel. After the signal is delivered from L_{panel} to L_{pen} , the mode of the panel transitions from the TX mode to the RX mode in order to receive the signal from the pen. The resonated signal of the pen is retransmitted from the pen to the panel in the RX mode of the panel. L_{panel} and C_{panel} are resonated by the magnetic field of L_{pen} and the SIG_2 signal is generated. By using the resonated signal from L_{panel} and C_{panel} , the read-out integrated circuit (IC) can detect the touch point. To achieve the constant resonance signal of the pen, it is important to transmit constant power in the TX. When the panel is fabricated in the factory, the resistances of each panel (R_{panel}) can have mismatches since it is difficult for panel manufacturers to make inductive coils in each panel exactly the same.

R_{panel} signifies the inherent resistance of the EMR panel. When it is fabricated by copper coil, as shown in Fig. 1, the width and the thickness of the copper coil vary. Since the resistances of the copper coils are determined by width and thickness, the copper coils have variations of resistance. The maximum mismatch between resistances of the EMR panel used in this paper is 10%. The panel and the pen are composed of inductors in this structure. The coupling coefficient between inductors is important when a signal is transmitted from the panel to the pen or vice versa. Ideally, the maximum value of the coupling coefficient is 1. To maximize the coupling coefficient, we increase the number of coils' winding in the pen and the panel. Although we increase the coupling coefficient as large as possible, the mismatches in the RX inputs are generated by the variation of

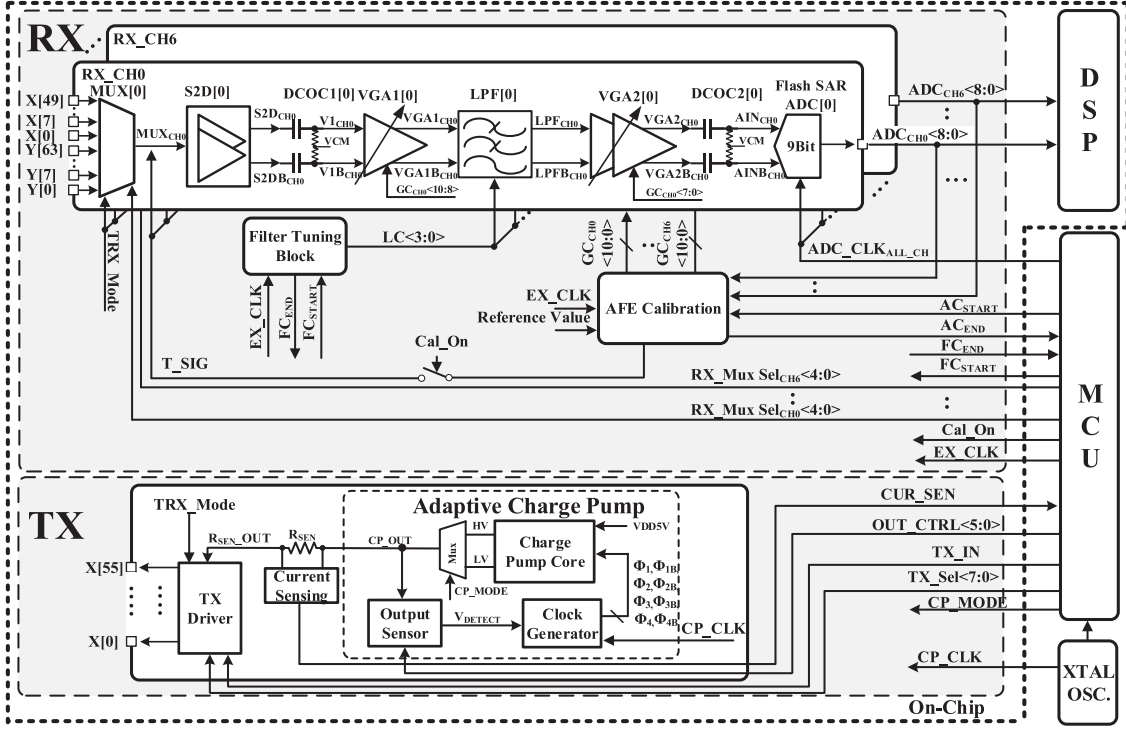


Fig. 3. Block diagram of the proposed AFE for the EMR touch panel.

the coupling coefficient. To block this effect, the RX can compensate for the signal of the RX using a calibration such as the gain of the VGA. The matching of L_{panel} and L_{pen} is not required. If L_{pen} is not coupled to L_{panel} , the received signal level is very small in the RX mode. On the contrary, the EMR occurs when L_{pen} is coupled to L_{panel} . Therefore, the coupling signal with L_{pen} is detected as a large signal when the application-specific integrated circuit (ASIC) is changed to the RX mode. Therefore, the ASIC can detect the channel where the coupling occurs, and the position of the pen is detected. If the signal is very large, the VGA gain is adjusted to prevent signal saturation. The TX driving frequency is about 500 kHz, and this AFE can drive up to a maximum frequency of 1 MHz. If the TX driving frequency is increased over 1 MHz, the transfer characteristics of the panel will be deteriorated, and a considerable amount of current consumption is also needed in the RX because the amplifiers demand large bandwidth to drive high frequency.

Fig. 3 presents a block diagram of the proposed AFE for the EMR touch panel. It is composed of a MUX, single-to-differential (S2D), DC offset cancellation circuits (DCOCs), the LPF, VGAs, the flash SAR ADC, the TX driver, and the adaptive charge pump. In order to attain a high speed when sensing the channel of the touch panel, the AFE for a multiple-path architecture is implemented. This structure can scan seven channels at the same time by switching the MUX. The X[55:0] in the touch panel is used as a transmitter and receiver channel. The Y[69:0] in the touch panel is used only as a receiver channel. It is possible to scan the entire channel by using only seven RXs because the microcontroller unit (MCU) controls the MUX.

The TX consists of the adaptive charge pump and the TX driver. The adaptive charge pump is proposed to compensate

for the difference of the resistance in the panel and to acquire uniformity of the SNR in each channel. If the resistance of the panel is high, the resonance is not generated because the current in the panel is not sufficient. If the resistance of the panel is low, a great deal of current is consumed in the panel. Therefore, in order to maintain a uniform current in each channel of the EMR panel, the adaptive charge pump is implemented. The TX driver transmits high power using the output of the adaptive charge pump. The push-pull structure that can drive the current is adopted as the TX driver to drive the current of the EMR touch panel because the inductive coil in the touch panel requires the current to operate.

The conventional touch system is composed of charge amplifiers and integrators to reduce noise and to amplify touch signals [12]–[14], [20]. As alternatives to charge amplifiers and integrators, an LPF and a VGA are adopted. To minimize the area of the RX for the on-chip, the VGA is designed to amplify the touch signal instead of the integrator. The magnitude of the transmitted signal from the pen to the panel is very small. To meet the input range of the ADC and fine resolution of calibration, two VGAs with different steps are designed to amplify the received signal at the panel. As the gain step of the VGAs gets finer, we can increase the resolution of the amplification and improve the accuracy of the calibration. The resolutions of the VGAs are designed to be about 4, 1, and 0.1 dB, respectively. If one VGA is designed to have a gain step of 0.1 dB, the area of the VGA will be large. Therefore, to compensate for the mismatches between AFEs effectively, we designed a coarse VGA with the gain step of 4 dB and a fine VGA with the gain step of 1 and 0.1 dB. Also, to adjust the gain finely in the gain calibration, a VGA with a resolution of 0.1 dB is designed. In order to implement the 0.1-dB step of the VGA, the amplifier

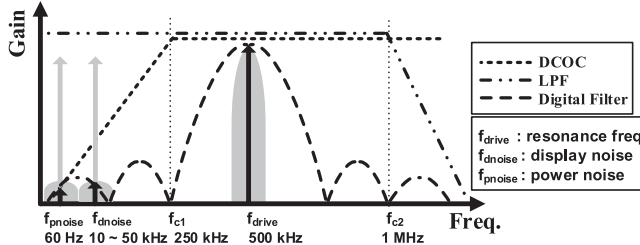


Fig. 4. Spectrum of touch signal and noises.

that has a high open-loop gain is designed for the VGA. The total gain of the three VGAs can vary between 0 and 44.5 dB. To implement the many functions in a single chip, this design includes the DSP. If they are implemented with the normal digital logic, the flexibility for various applications can be limited. Thus, the DSP is adopted for implementing digital filters and detecting position for several smartphone applications flexibly.

Fig. 4 shows the spectrum of the touch signal and noises. In electronic devices, the touch sensor is located on the display.

Since display noise can affect the performance of the touch sensor, a differential sensing scheme, S2D, a DCOC, and a digital filter are adopted. The S2D is designed for differential signaling to reject noise from the panel. In addition, the digital filter in the DSP is implemented to reduce noise. Furthermore, the operation frequency of 500 kHz is adopted to avoid display noise that has a frequency under 100 kHz. The LPF with the cutoff frequency of 1 MHz is implemented to reject high-frequency noise. Even though the S2D can be vulnerable to the display noise, EMR between the panel and the pen can provide the sharp filtering characteristics before the S2D rejecting the display noise partially. In addition, the resonance frequency (f_{drive}), which is far from the display noise band, is used to prevent saturation of the signal. High-frequency noise is attenuated by the LPF and low-frequency noise is attenuated by the DCOC and the digital filter in the DSP. The attenuation characteristic is determined by each block. To acquire a low system noise figure (NF), the S2D is designed to have the gain. Thus, external noises such as display noise and charger noises can be rejected by the differential processing, an analog LPF, and digital filters in the DSP. The S2D is used to generate a differential signal because it is more robust than single-ended signaling [21]. The DCOC has two functions that redefine the voltage common mode (VCM) level to avoid signal distortion and rejects low-frequency noise. It can also solve the problem of DC offset and DC wandering. In order to reduce the error when the analog signal is converted to digital, the DCOC is inserted in front of the ADC. The LPF is implemented in the AFE in order to reject the noise from the touch panel. If the charge amplifier is directly connected to the touch panel, the capacitor of the charge amplifier can affect the resonance in the EMR touch panel. Unlike conventional filters, the proposed filter has a filter tuning circuit, which is included to maintain the characteristics of the filter due to process and environmental variations of resistances and capacitances. The characteristics of the LPF in the AFE are almost constant, thanks to the filter tuning, and the mismatches between the seven RXs can be minimized by calibration in the initial period.

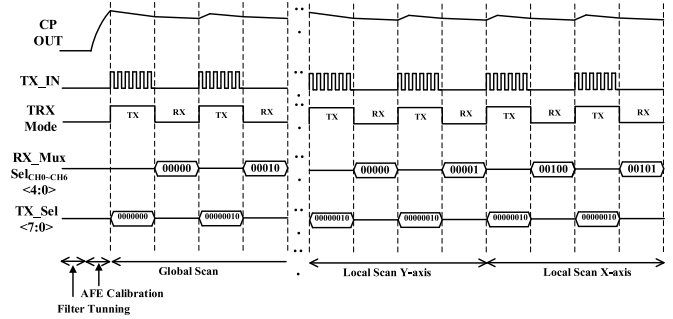


Fig. 5. Timing diagram of the AFE.

Therefore, during the touch signal processing, the mismatches between the AFEs can be neglected. While designing the ADC, the sampling rate and the area are considered. The sampling rate of the flash ADC is faster than that of the SAR ADC, and the area of the SAR ADC is smaller than the area of the flash ADC. Therefore, to acquire the advantage of both the flash and SAR, the combined flash SAR ADC is proposed in the AFE. In general, while the SAR ADC has the advantages of high resolution and a simple circuit, the high sampling rate is limited and the area is large because of the capacitors. The flash ADC has a high speed [22], but it is difficult to design a resolution over 8 bit. In order to acquire these advantages, the flash SAR ADC is proposed. Within the available area on the chip, a 6-bit is selected as the SAR ADC and a 3-bit flash ADC is proposed for the 9-bit Flash SAR ADC. The calibration is operated in the initial period to compensate for the mismatch by adjusting the gain of the VGA. After the calibration, all seven RXs have similar characteristics around the same signal. The VGA is applied to reduce the required ADC resolution.

Fig. 5 presents the timing diagram of the AFE. The TX and RX modes are dependent on the MCU control signal. Initially, before scanning the touch panel, the filter tuning, AFE calibration, and the adaptive charge pump is operated. The MCU switches the MUX to scan the channels of the touch panel. The global scan begins to scan the channels before the local scan. If a signal is detected by the RX when operating the global scan mode, the local scan is started. The local scan is operated for only 14 channels near the large signal when the mode is in the global scan. The pen is detected after the scan of the X-axis and Y-axis local scan has finished. By using the global scan and the local scan, we can efficiently detect the pen on the touch panel.

III. PROPOSED AFE ARCHITECTURE FOR AN EMR TOUCH PANEL

A. Adaptive Charge Pump

Fig. 6(a) shows a block diagram of the adaptive charge pump. The charge pump has the advantages of a small area and low power consumption compared to the dc-dc converter. The charge pump is selected instead of the dc-dc converter because only one channel is driven among several channels when transmitting the signal to the touch panel. Also, the output of the proposed adaptive charge pump is either the high-voltage (HV) or low-voltage (LV) mode by the MCU. The selection is made

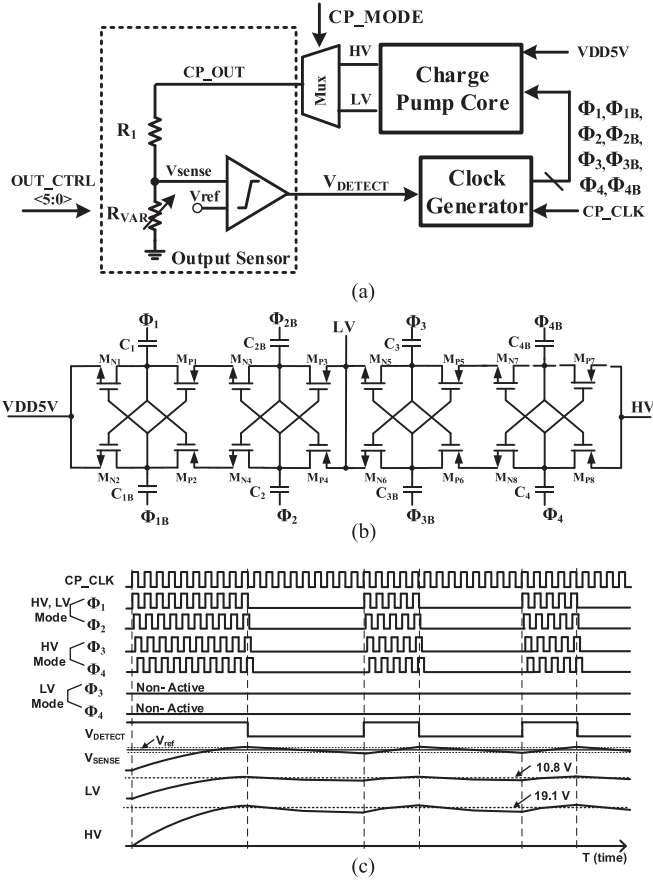


Fig. 6. (a) Block diagram, (b) core, and (c) timing diagram of the adaptive charge pump.

to the requirements of the SNR and low power performance. If the SNR is required, the charge pump operates in the HV mode. On the other hand, it operates in the LV mode when the performance of low power is important. The EMR panel needs a uniform current in each channel because it is the inductive coil panel. Because each channel of the panel has a different resistance, the adaptive charge pump controls the output voltage to maintain the current in each channel. Many kinds of panels exist in the field of touch screens. Some panels have low resistance and other panels have high resistance such as the one used in this study. To apply the proposed design to various panels, the adaptive charge pump is designed. The proposed adaptive charge pump is scalable in order to drive the various resistances of the touch panel. If the touch panel has high resistance, the current in the touch panel is insufficient. In this case, it needs to increase the adaptive charge pump voltage. If the touch panel has low resistance, the current consumption is high. It needs to decrease adaptive charge pump voltage. Therefore, this adaptive charge pump operates efficiently for various touch panels.

Fig. 6(b) shows the charge pump core. In this paper, the Dickson charge pump is used because of its ability to generate a voltage that is higher than the input voltage [23]–[25]. This circuit is composed of HV MOSFETs and capacitors. As the MOSFETs are turned ON or OFF, each capacitor is charged and the output voltage is boosted to the HV. Signals Φ_1 , Φ_2 , Φ_3 , and Φ_4 have four phases, while Φ_{1B} , Φ_{2B} , Φ_{3B} , and Φ_{4B} have differential

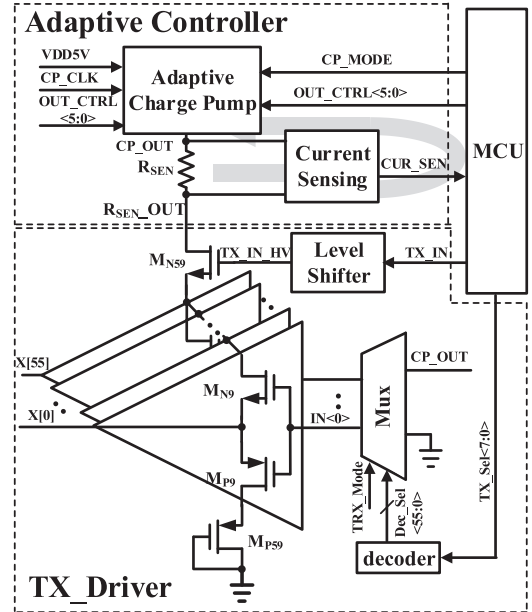


Fig. 7. Block diagram of the TX driver with an adaptive controller.

phases. If the clocks are generated at same phase, the MOSFETs between the neighboring stages are ON at the same time. The charge is moved to a reverse direction because of the potential difference, and the adaptive charge pump efficiency is decreased. Therefore, in order to operate the adaptive charge pump efficiently, four phase clocks are needed. The LV is needed for low resistance and the designed adaptive charge pump is operated in the LV mode. In the LV mode, only two stages of the adaptive charge pump core are used to generate low output voltage because the use of two stages is more efficient than four stages.

Fig. 6(c) provides the timing diagram of the adaptive charge pump. In the HV mode, Φ_1 , Φ_2 , Φ_3 , and Φ_4 are used. On the other hand, Φ_1 and Φ_2 are used only to optimize the power consumption. The output voltages are 10.8 and 19.1 V in the LV and HV modes, respectively.

B. TX Driver With an Adaptive Controller

Fig. 7 shows the block diagram of the TX driver with an adaptive controller. The EMR touch panel needs to be able to drive a large amount of current because the structure of this touch panel is an inductive coil. In order to drive the EMR touch panel, a push-pull-type structure is implemented. M_{N59} and M_{P59} are not needed at each channel because only one channel is selected when the signal is transmitted to the touch panel. Therefore, since the TX driver with an adaptive controller is designed, as shown in Fig. 6, we can reduce the area of HV MOSFETs occupied on the chip and drive the EMR touch panel. The proposed design has a current-sensing block to detect the current of the EMR panel. As the signal of the current sensing is delivered to the MCU, it controls the output of the charge pump adaptively according to the current-sensing block. Therefore, through the adaptive controller, the push-pull driver can provide the same current in each channel regardless of the mismatches in the resistances of each channel.

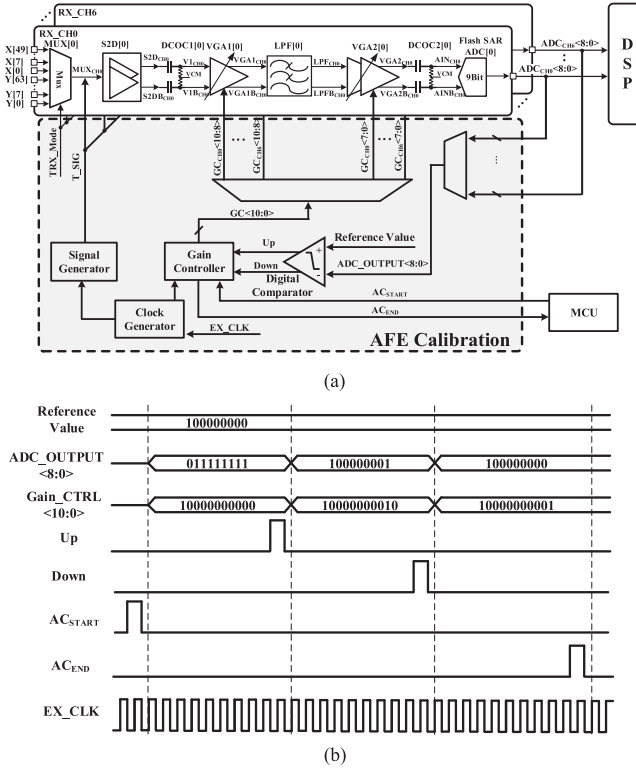


Fig. 8. (a) Block diagram and (b) timing diagram of the AFE calibration.

C. VGA With an AFE Calibration

Fig. 8(a) demonstrates the block diagram for the AFE calibration, which is enabled at the initial power up time. It is composed of 4-, 1-, and 0.1-dB resolution VGAs and AFE calibration. After finishing the calibration, it is disabled to lessen power consumption. The T_SIG is applied to the MUX_{CH0} and the ADC_{CH0<8:0>} is checked by the AFE calibration block, which adjusts the GC_{CH0<10:0>} to acquire the same code of ADC output because T_SIG is the same signal sent to seven AFEs.

The receiver is composed of VGA1, LPF, and VGA2. The blocks are located to improve the SNR, as shown in Fig. 8. To increase the SNR, the cascaded NF in the receiver should be improved. In the cascaded system, an improved NF can be achieved when the high-gain low-noise block is located in the front rather than low-gain block such as the LPF. Therefore, when the VGA1 with a large gain and low noise is located in front of the AFE, the total NF of the AFE is improved. If the low-gain VGA is located in front of the AFE, the total NF is degraded based on the equations of the cascaded NF [26]. After the AFE calibration detects the digital output of the flash SAR ADC, it automatically controls GC_{CH0<10:0>} to change the gain of the VGA. The total dynamic gain range is from 0 to 44.5 dB, and the gain step is 0.1 dB.

Fig. 8(b) shows the timing diagram of the AFE calibration. The optimization process is as follows. First, T_SIG is applied to the input of RX in Fig. 3. Then, the data from the ADC are scanned, and the input signal amplitude can be checked. In the AFE calibration block, the VGA gain is adjusted until it becomes the desired signal amplitude to find the optimized

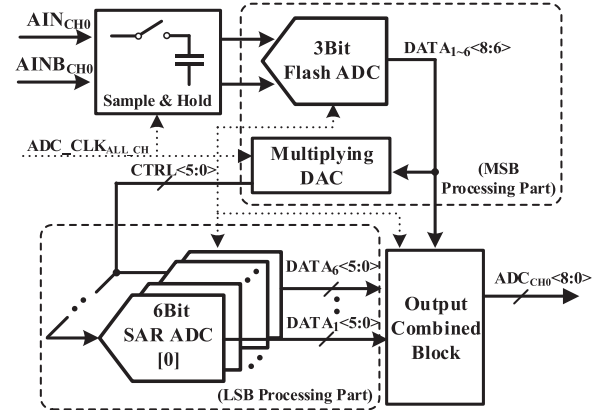


Fig. 9. Block diagram of the 9-bit flash SAR ADC.

gain value. After comparing the ADC_OUTPUT<8:0> with the reference value, the up and down signals are generated. If the ADC_OUTPUT<8:0> is the same as the reference value, the calibration is stopped and the gain settings are delivered to the VGAs.

D. Combined Flash SAR ADC

Fig. 9 shows the concept of the flash SAR ADC. The designed structure for the ADC is composed of a 3-bit flash ADC and a 6-bit SAR ADC. The sampled input signal is processed by the flash ADC. The flash ADC generates 3-bit during each CLK period, and the multiplying digital-to-analog converter (MDAC) is operated by 3-bit. The output voltage of the MDAC is delivered to the input of the SAR ADC and the output of the SAR is released from the most significant bit (MSB). The MDAC is operated to residue process by using the 3-bit output of the flash ADC. Because the driving frequency is under 1 MHz in this application, the sampling rate of 2 MS/s is adopted to avoid the aliasing based on the Nyquist theory [27]. The 3-bit flash ADC is composed of a resistor ladder, comparators, and a 3-bit encoder [28]. The flash ADC selects three MSBs in 9-bit. The 6-bit SAR ADC consists of a comparator, capacitors, and SAR logic. The output of the comparator is determined by switching the capacitors [27]. After the differential input is sampled, the digital output is released following the SAR logic. The output combined block is used to combine the code of the flash ADC with the code of the SAR ADC. The MSB is selected by the flash ADC and the least significant bit (LSB) is released from the SAR ADC.

IV. EXPERIMENTAL RESULTS

This chip is implemented in a 0.18- μm BCD process. Fig. 10 illustrates the designed chip microphotograph of the AFE for the touch panel. The AFE is placed symmetrically on the chip. The MUX is located near the pad to reduce the distance of the channel and each block has a guard ring to reject noise. The chip area is 40 mm² including the DSP. The TX area is relatively large since HV devices are used for the adaptive charge pump.

Fig. 11 shows the measurement test board for the AFE. It is composed of the MCU, a supply port, and a touch panel connector to verify the performance of the AFE for the touch

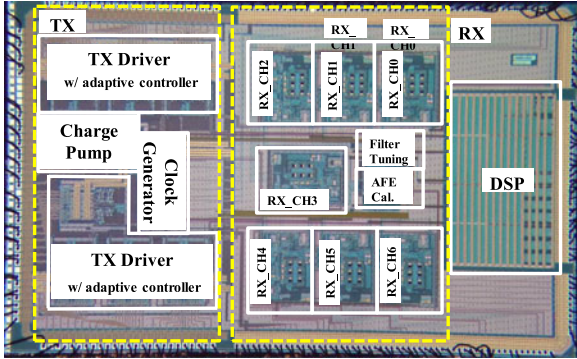


Fig. 10. Chip microphotograph.

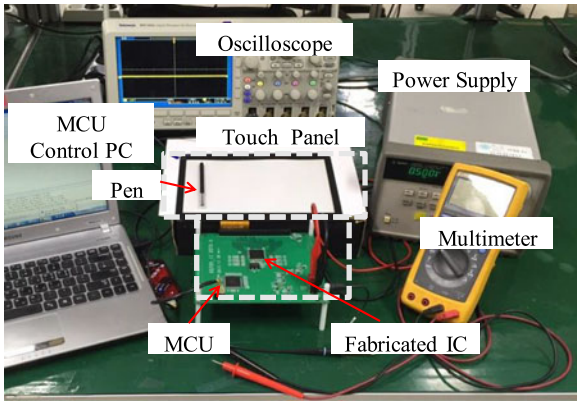


Fig. 11. Measurement environment.

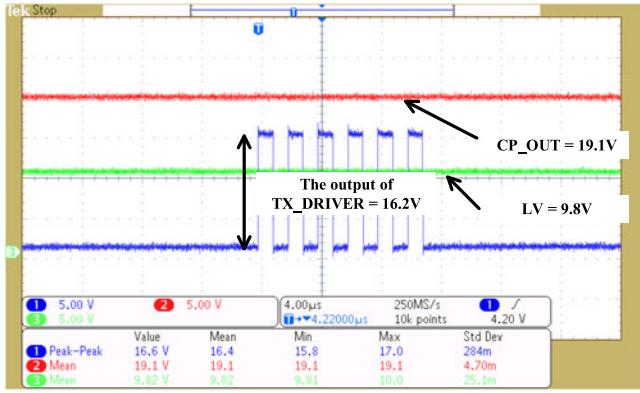


Fig. 12. Measurement of an adaptive charge pump and the TX driver.

panel. Using the external MCU, the data from the fabricated IC are acquired, and the data are analyzed by the MCU control PC. The fabricated IC processes the signal from the touch panel and the MCU controls the fabricated IC. The size of the target touch panel is 10.1 in. The measurement includes only the touch panel and not the display panel. Also, the transparent electrode type is the inductive coil. The electrode material is composed of copper and the one-channel resistance is 300 Ω per channel.

Fig. 12 provides the measurement results of the adaptive charge pump and the output of the TX driver. The adaptive charge pump generates 19.1 V by pumping capacitors. The TX driver generates an HV signal by using the output of the

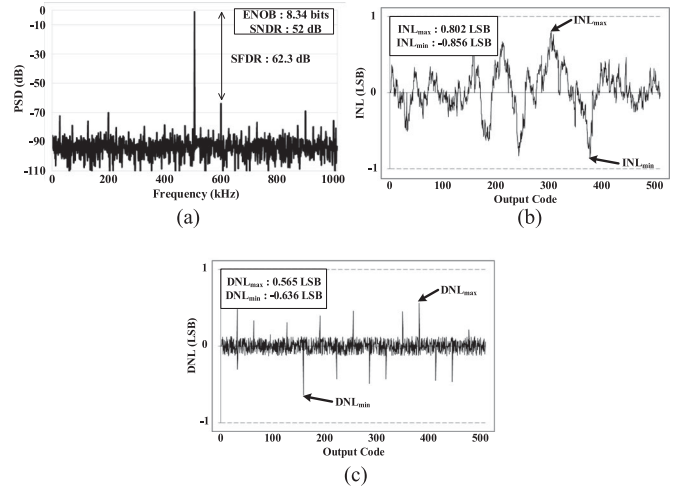


Fig. 13. Combined flash SAR ADC measurement result. (a) Effective number of bits. (b) Integral nonlinearity. (c) Differential nonlinearity.

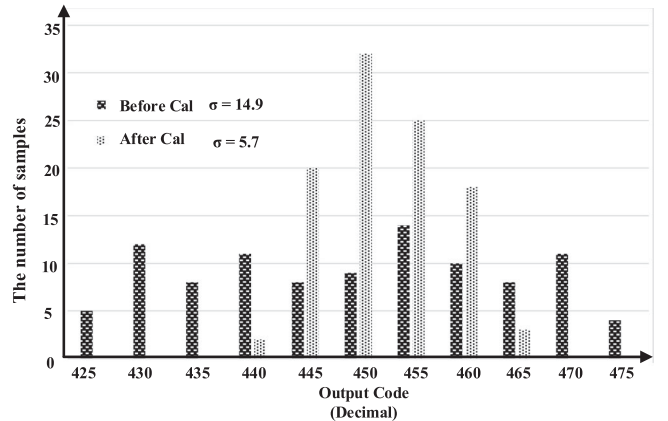


Fig. 14. AFE calibration measurement result.

adaptive charge pump. The voltage level of the output swing is 16.2 V. Fig. 13(a) shows the measured spectrum of the ADC output. The measured effective number of bits (ENOB), signal to noise plus distortion ratio (SNDR), and spurious free dynamic range (SFDR) are 8.34 bits, 52 dB, and 62.3 dB, respectively. The maximum and minimum integral non-linearity (INL) values are 0.802 LSB and -0.856 LSB, respectively, as shown in Fig. 14(b). Fig. 14(c) shows that the maximum and minimum differential non-linearity (DNL) are 0.565 LSB and -0.636 LSB, respectively.

Fig. 14 shows the AFE calibration measurement results. This histogram represents the difference between before and after calibration. The X- and Y-axes present the output code of the flash SAR ADC and the number of samples, respectively. Before calibration, the maximum difference is about 50 codes of the flash SAR ADC. After calibration, the variation between the maximum and minimum codes is about 25 ADC codes. The standard deviation is reduced from 14.9 to 5.7 as a result of the calibration.

Fig. 15 shows the relationship between the SNR and the TX power in Fig. 2(b) driven by the TX in the panel. The TX power is proportional to the output voltage of the adaptive charge pump

TABLE I
PERFORMANCE OF AFE FOR THE TOUCH PANEL

Touch panel type	[12] Mutual Capacitive	[13] Mutual Capacitive	[20] Mutual Capacitive	[32] Mutual Capacitive	[33] Mutual Capacitive	This work Inductive Coil
Channel	TX: 48 RX: 32	TX: 80 RX: 80	TX: 12 RX: 16	TX: 28 RX: 16	TX: 78 RX: 138	TRX: 56 RX: 70
Technology	BCD 0.18 μ m	CMOS 0.35 μ m	CMOS 0.35 μ m	CMOS 90 μ m	CMOS 0.18 μ m	BCD 0.18 μ m
SNR	49 dB	32 dB	27.5 dB	42 dB	37 dB	39.5 dB
Frame Rate	120 Hz	322 Hz	175 Hz	120 Hz	240 Hz	300 Hz
The number of scan channel (channel/s)	3840	25 760	5250	1920	33 120	37 800
Supply Voltage	3 V	N. A.	3.3 V	1.2 V, 3.3 V, 12 V	1.8 V, 3.3 V	1.8 V, 5 V
Sampling Rate	N. A.	N. A.	100 kS/s	N. A.	N. A.	2 MS/s
Power Consumption	30 mW	21.8 mW	76 mW	24.6 mW	559.9 mW	110 mW (TX: 65 mW RX: 45 mW)
Chip Area	14.7 mm ² (w/o DSP, ADC)	6.25 mm ² (w/o DSP)	5.02 mm ² (w/o DSP, ADC)	15.9 mm ² (w/o DSP, ADC)	71.2 mm ² (w/ DSP, ADC)	40 mm ² (w/ DSP, ADC)

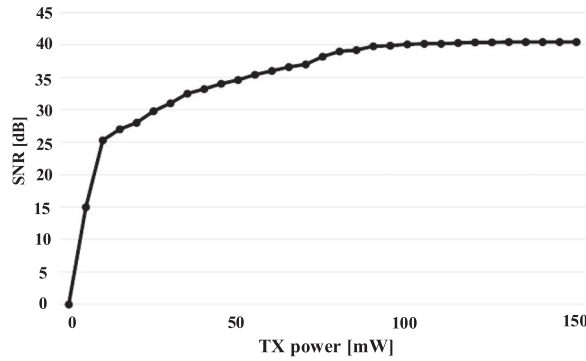


Fig. 15. Measured SNR with respect to TX power in the panel.

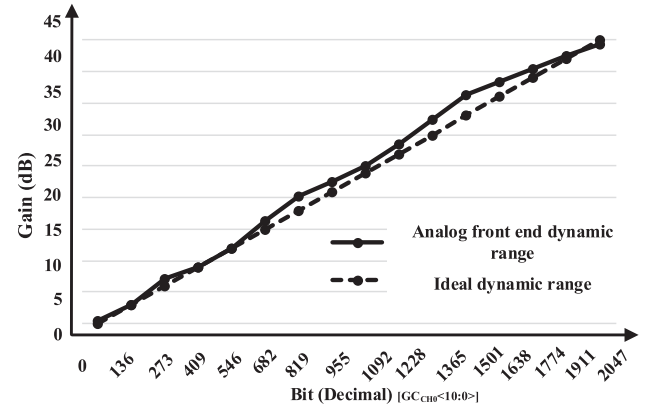


Fig. 16. Dynamic gain range of the AFE measurement result.

in the TX. Therefore, if the output voltage level of the adaptive charge pump is low, the load current and delivered signal (SIG_2) in Fig. 2(b) will be reduced. As shown in Fig. 15, when the TX power is 6.75 mW, the SNR is decreased abruptly because the load current is not enough. In addition, if the load current is greater than 87.48 mW, the SNR will be almost constant. Therefore, the load current is determined to be about 54 mA in order to minimize the current consumption and achieve the desired SNR. The TX power consumption in Table I signifies average power consumption including the current consumption of the EMR panel and Tx in the chip. The power consumption means the active power consumption when driving the EMR panel, as shown in Fig. 15.

The inductive coupling method is adopted in this application. The inductor components in this module have their own power losses due to the parasitic series resistances, which cause the power losses of the transmitted signal at the EMR panel and the resonated signal at the pen. Thus, the SNR is limited even though the TX power is increased. Fig. 16 shows the dynamic gain range of the AFE. The resolution of the AFE is designed as a 0.1-dB step to compensate for a minor mismatch. The maximum dynamic range is 45 dB. The display noise ranged from 10 to 50 kHz, as shown Fig. 4.

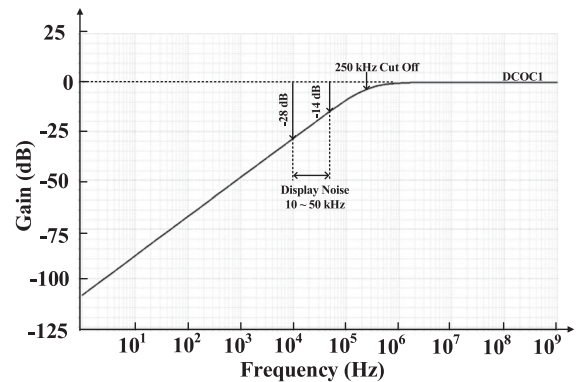


Fig. 17. Simulation result of DCOC.

Fig. 17 provides the simulation result of the DCOC1. The display noise is attenuated more than 14 dB by one stage of the DCOC. The RX has two DCOC stages, as shown Fig. 2. Therefore, the display noise can be attenuated more than 28 dB from 10 to 50 kHz. Fig. 18 shows the SNR measurement result of the proposed AFE. The SNR for touch panel application is

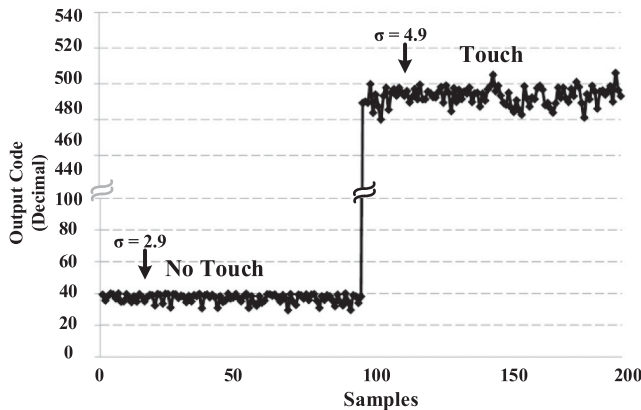


Fig. 18. SNR measurement result.

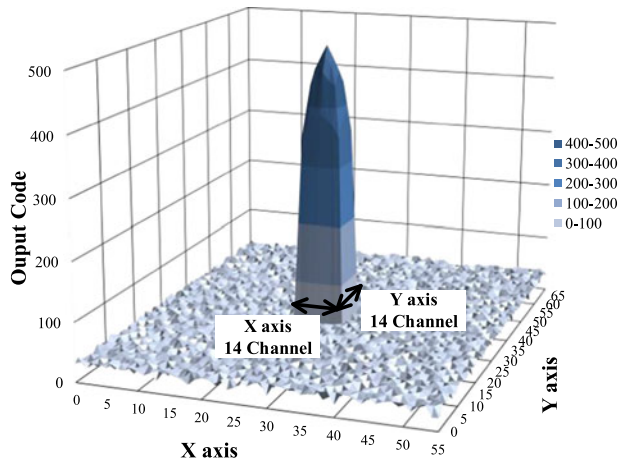


Fig. 19. Pen touch image.

calculated as follows [29]–[31]:

$$\text{SNR} = 20 \times \log \frac{|M_N - M_T|}{\sigma} \quad (1)$$

where

M_N mean value when not touched;

M_T mean value when touched;

σ standard deviation when touched.

The X - and Y -axes represent the number of samples and the output code of the Flash SAR ADC, respectively. In order to acquire the SNR, the mean values of touch and no touch are calculated. In addition, the standard deviation of noise with touch is calculated. By subtracting the average with no touch from the average with touch and dividing this result by the standard deviation of noise with touch, the SNR is acquired.

Fig. 19 shows an image of the pen touch. It presents the ADC's output code value of each X and Y channels when the EMR pen is touched to the panel. The touched position has the maximum value, and this system can determine the touch point after obtaining the code value at each channel.

The touch spot is detected by measuring the output code of the ADC. Table I shows the performance summary of the proposed pen detection analog system for the 56×70 channel EMR touch panel. Since there are no prior published studies for the

EMR touch panel as far as we know, performance comparison with those for other panel types is added in Table I instead of the EMR touch panel. [12], [13], [20], [32], and [33] are touch systems using a capacitive touch panel. Because the systems in the references are implemented for the human finger, limitations arise for the pen detection applications. They can cause the inaccurate touched data when people use the pen in the touch panel. In the EMR pen touch system, the quality and brightness of the display screen are not degraded and the panel is not touched directly because the touch panel is located behind the display screen. Therefore, the durability of the touch panel is extremely high. In addition, it is possible to detect even small characters written using the pen because the EMR touch panel has high precision and high resolution [11]. As the several AFE paths are implemented, it can drive many channels in the EMR touch panel and acquire a high frame rate contrary to the conventional structures for touch panels [12]–[17]. The chip area of this work is larger than those of [12], [13], [20], and [32], since the ADC and DSP are not included in the fabricated chips used by those references. Also, because this work is targeting the EMR panel application requiring much current, the large HV DMOSs are used for the adaptive charge pump and occupy a larger area than those of [12], [13], [20], and [32]. Because the EMR inductive coil used in this work requires larger currents compared with [12], [13], [20], [32], and [33], the current consumption of this work is relatively large. However, the SNR of this work is the best except [12] and [32]. Therefore, the proposed structure has a frame rate of 300 Hz to scan the 56×70 channel EMR touch panel. In addition, the number of channels per second is greater than those of [12], [13], [20], [32], and [33]. As the VGAs are used instead of integrators in the AFE, the die area is reduced. In addition, a high-resolution VGA is proposed to compensate for the mismatches between the seven paths of the receiver with the AFE calibration, and it can maintain the uniformity of the SNR across the seven paths.

V. CONCLUSION

In this paper, the pen detection AFE for the EMR touch panel was presented. The adaptive charge pump was implemented to transmit an HV signal and compensated the resistance of the touch panel. The AFE was designed with a seven-path architecture to scan many channels quickly in parallel. The ADC was combined with the flash SAR ADC to increase the sampling rate and reduce the area. The obtained SNR was about 39.5 dB in this AFE, and the frame rate was about 300 Hz with the 56×70 touch panel. The proposed design was implemented in a $0.18\text{-}\mu\text{m}$ BCD process. The chip area was 40 mm^2 including the DSP and ADC. The power consumption of TX and RX excluding the DSP and MCU was 65 and 45 mW, respectively.

REFERENCES

- [1] T.-H. Hwang, W.-H. Cui, I.-S. Yang, and O.-K. Kwon, "A highly area-efficient controller for capacitive touch screen panel systems," *IEEE Trans. Consum. Electron.*, vol. 56, no. 2, pp. 1115–1122, May 2010.
- [2] J. Lee, "Picture-based address power saving method for high resolution plasma display panel (PDP)," *IEEE Trans. Ind. Electron.*, vol. 55, no. 1, pp. 49–58, Jan. 2008.

- [3] J. Won, H. Ryu, T. Delbruck, J. Lee, and J. Hu, "Proximity sensing based on a dynamic vision sensor for mobile devices," *IEEE Trans. Ind. Electron.*, vol. 62, no. 1, pp. 536–544, Jan. 2015.
- [4] J.-S Wang, Y.-L. Hsu, and J.-N Liu, "An inertial measurement unit based pen with a trajectory reconstruction algorithm and its applications," *IEEE Trans. Ind. Electron.*, vol. 57, no. 10, pp. 3508–3520, Oct. 2010.
- [5] J.-S Wang and J.-N Liu, "An accelerometer-based digital pen with a trajectory recognition algorithm for handwritten digit and gesture recognition," *IEEE Trans. Ind. Electron.*, vol. 59, no. 7, pp. 2998–3007, Jul. 2012.
- [6] A. Hughes, "Active pen input and the android input framework," M.S. thesis, Dept. Elect. Eng., California Polytech State Univ., San Luis Obispo, CA, USA, 2011.
- [7] J. An *et al.*, "A 3.9 kHz-frame-rate capacitive touch system with pressure/tilt angle expressions of active stylus using multiple-frequency driving method for 65" 104 × 64 touch screen panel," in *Proc. IEEE Int. Solid-State Circuits Conf.*, Feb. 2017, pp. 168–169.
- [8] C.-L. Lin *et al.*, "Tracking touched trajectory on capacitive touch panels using adjustable weighted prediction covariance matrix," *IEEE Trans. Ind. Electron.*, vol. 64, no. 6, pp. 4910–4916, Jun. 2017.
- [9] R. B. Mudit and V. B. Anand, "Comparative study of various touchscreen technologies," *Int. J. Comput. Appl.*, vol. 6, no. 8, pp. 12–18, Sep. 2010.
- [10] G. Walker and M. Fihm, "LCD in-cell touch," *Inf. Display*, Mar. 2010, pp. 8–14.
- [11] Wacom, EMR Technology. 2015. [Online]. Available: <http://www.wacom-components.com/english/technology/index.html>
- [12] C. Park *et al.*, "A pen-pressure-sensitive capacitive touch system using electrically coupled resonance Pen," in *Proc. IEEE Int. Solid-State Circuits Conf.*, Feb. 2015, pp. 1–3.
- [13] N. Miura *et al.*, "A 1 mm-pitch 80 × 80-channel 322 Hz-frame-rate touch sensor with two-step dual-mode capacitance scan," in *Proc. IEEE Int. Solid-State Circuits Conf.*, Feb. 2014, pp. 216–217.
- [14] H. Shin, S. Ko, H. Jang, I. Yun, and K. Lee, "A 55 dB SNR with 240 Hz frame scan rate mutual capacitor 30 × 24 touch-screen panel read-out IC using code-division multiple sensing technique," in *Proc. IEEE Int. Solid-State Circuits Conf.*, Feb. 2013, pp. 388–389.
- [15] J. Park, D. Lim, and D. Jeong, "A Reconfigurable 40-to-67 dB SNR, 50-to-6400 Hz frame-rate, column-parallel readout IC for capacitive touch-screen panels," *IEEE J. Solid-State Circuits*, vol. 49, no. 10, pp. 2305–2318, Feb. 2014.
- [16] S. Pietri, A. Olmos, M. Berens, A. Vilas Boas, and M. Goes, "A fully integrated touch screen controller based on 12b 825kS/s SAR ADC," in *Proc. IEEE Argentine School Micro-Nanoelectron., Technol. Appl.*, Oct. 2009, pp. 66–70.
- [17] I. F. I. Albittar, J. Kim, and H. Kim, "The design of 13 bits $\Sigma\Delta$ ADC for a mutual-capacitance large touch screen controller," in *Proc. Int. SoC Des. Conf.*, Nov. 2014, pp. 108–109.
- [18] P. K. Chu, *Advances in Solid State Circuit Technologies*. Rijeka, Croatia: InTech, 2010.
- [19] C. R. Paul, *Inductance: Loop and Partial*, 1st ed. New York, NY, USA: Wiley, 2009.
- [20] J. Lee, D. Yeo, H. Kwon, B. Kim, J. Sim, and H. Park, "An LCD-VCOM-noise resilient mutual-capacitive touch-sensor IC chip with a low-voltage driving signal," *IEEE Sens. J.*, vol. 15, no. 8, pp. 4595–4602, Aug. 2015.
- [21] B. Razavi, *Design of Analog CMOS Integrated Circuits*. New York, NY, USA: McGraw-Hill, Mar. 2010.
- [22] K. Balasubramanian, "A Flash ADC with reduced complexity," *IEEE Trans. Ind. Electron.*, vol. 42, no. 1, pp. 49–58, Feb. 1995.
- [23] M.-D. Ker, S.-L. Chen, and C.-S. Tsai, "Design of charge pump circuit with consideration of gate-oxide reliability in low-voltage CMOS processes," *IEEE J. Solid-State Circuits*, vol. 41, no. 5, pp. 1100–1107, May 2006.
- [24] M. Hoque, T. McNutt, J. Zhang, A. Mantooth, and M. Mojarradi, "A high voltage Dickson charge pump in SOI CMOS," in *Proc. IEEE Custom Integr. Circuits Conf.*, Sep. 2003, pp. 493–496.
- [25] X. Zhang and H. Lee, "An efficiency-enhanced auto-reconfigurable 2x/3x SC charge pump for transcutaneous power transmission," in *Proc. IEEE Custom Integr. Circuits Conf.*, Sep. 2009, pp. 311–314.
- [26] T. H. Lee, *The Design of CMOS Radio-Frequency Integrated Circuit*, 2nd ed. Cambridge, U.K.: Cambridge Univ. Press, Jan. 1998.
- [27] P. E. Allen and D. R. Holberg, *CMOS Analog Circuit Design*, 3rd ed. Oxford, U.K.: Oxford Univ. Press, Mar. 1987.
- [28] B. Kim, L. Yan, J. Yoo, N. Cho, and H. Yoo, "An energy-efficient dual sampling SAR ADC with reduced capacitive DAC," in *Proc. IEEE Int. Symp. Circuits Syst.*, May 2009, pp. 972–975.
- [29] S. Ko *et al.*, "Low noise capacitive sensor for multi-touch mobile handset's applications," in *Proc. IEEE Asian Solid State Circuits Conf.*, Nov. 2010, pp. 1–4.
- [30] *Techniques for Robust Touch Sensing Design*, Microchip Technology Inc., Chandler, AZ, USA, 2010–2013.
- [31] *Touch Sensors Design Guide*, ATMEL Corp., San Jose, CA, USA, 2008–2009.
- [32] K. Kim *et al.*, "A fully-differential capacitive touch controller with input common-mode feedback for symmetric display noise cancellation," in *Proc. Symp. VLSI Circuits*, Jun. 2014, pp. 1–2.
- [33] M. Hamaguchi, A. Nagao, and M. Miyamoto, "A 240 Hz-Reporting-rate 143×81 mutual-capacitance touch-sensing analog front-end IC with 37 dB SNR for 1mm-diameter stylus," in *Proc. IEEE Int. Solid-State Circuits Conf.*, Feb. 2014, pp. 214–215.



SangYun Kim received the B.S. degree in electronic engineering from Konkuk University, Seoul, South Korea, in 2013. He is currently working toward the combined M.S./Ph.D. degree at the College of Information and Communication Engineering, Sungkyunkwan University, Suwon, South Korea.

His research interests include high-speed interface integrated circuits and CMOS radio frequency transceivers.



SungHun Cho (S'13) received the B.S. degree in electronic engineering from Hongik University, Seoul, South Korea, in 2013, and the M.S. degree in electronic engineering from Sungkyunkwan University, Suwon, South Korea, in 2015, where he is currently working toward the Ph.D. degree at the School of Information and Communication Engineering.

His research interests include CMOS radio frequency transceivers and automotive integrated circuit design.



YoungGun Pu received the B.S., M.S., and Ph.D. degrees in electronic engineering from Konkuk University, Seoul, South Korea, in 2006, 2008, and 2012, respectively.

His research interests include CMOS fully integrated frequency synthesizers and oscillators and transceivers for low-power mobile communication.



Sang-Sun Yoo (M'15) received the B.S. degree from the Department of Semiconductor Science, Dong-guk University, Seoul, Korea, in 2004, and the M.S./Ph.D. degree from the Department of Information and Communication Engineering, Korea Advanced Institute of Science and Technology (KAIST), Daejeon, in 2012.

He was with the System LSI Division, Samsung Electronics, from 2012 to 2015 where he focused on ADPLL for 3/4G mobile applications as a Senior Design Engineer. From 2015 to 2016,

he was a Research Assistant Professor in KAIST and Sungkyunkwan University. Since 2017, he has been with Department of Smart Automobile, Pyeongtaek University, where he is currently an Assistant Professor. His research interests include RF systems for mobile communications, reconfigurable RFICs, automotive ICs, ADPLL, RFID, and sensor communications.

Dr. Yoo was the recipient of the Best Paper Award of the IEEE TRANSACTIONS ON INDUSTRIAL ELECTRONICS in 2011.



Minjae Lee was born in 1976. He received the B.Sc. and M.S. degrees from Seoul National University, Seoul, South Korea, in 1998 and 2000, respectively, and the Ph.D. degree from the University of California, Los Angeles, CA, USA, in 2008, all in electrical engineering.

In 2000, he was a Consultant with GCT semiconductor, Inc., and Silicon Image Inc., designing analog circuits for wireless communication and digital signal processing blocks for Gigabit Ethernet. He joined Silicon Image Inc., Sunnyvale, CA, in 2001, developing Serial ATA products. In August 2008, he joined Agilent Technologies, Santa Clara, CA, where he was involved with the development of next-generation high-speed analog-to-digital converters and digital-to-analog converters. Since 2012, he has been with the School of Information and Communications, Gwangju Institute of Science and Technology, Gwangju, South Korea, where he is currently an Assistant Professor.

Dr. Lee received the Best Student Paper Award at a Symposium in Kyoto, Japan, in 2007 and the GIST Distinguished Lecture Award in 2015.



Younghoo Yang was born in Hamyang, South Korea, in 1969. He received the Ph.D. degree in electrical and electronic engineering from Pohang University of Science and Technology, Pohang, South Korea, in 2002.

From 2002 to 2005, he was with Skyworks Solutions Inc., Newbury Park, CA, USA, where he designed power amplifiers for various cellular handsets. Since March 2005, he has been with the School of Electronic and Electrical Engineering, Sungkyunkwan University, Suwon, South Korea, where he is currently a Professor. His research interests include radio frequency (RF)/millimeter-wave power amplifiers, RF transmitters, envelope tracking supply modulator integrated circuits, and wireless power transfer technologies.



Keum Cheol Hwang (SM'13) received the B.S. degree in electronics engineering from Pusan National University, Busan, South Korea, in 2001, and the M.S. and Ph.D. degrees in electrical and electronic engineering from Korea Advanced Institute of Science and Technology, Daejeon, South Korea, in 2003 and 2006, respectively.

From 2006 to 2008, he was a Senior Research Engineer with Samsung Thales, Yongin, South Korea, where he was involved with the development of various antennas including multiband fractal antennas for communication systems and Cassegrain reflector antenna and slotted waveguide arrays for tracking radars. He was an Associate Professor in the Division of Electronics and Electrical Engineering, Dongguk University, Seoul, South Korea, from 2008 to 2014. In 2015, he joined the Department of Electronic and Electrical Engineering, Sungkyunkwan University, Suwon, South Korea, where he is currently an Associate Professor. His research interests include advanced electromagnetic scattering and radiation theory and applications, design of multiband/broadband antennas and radar antennas, and optimization algorithms for electromagnetic applications.

Prof. Hwang is a Life Member of the Korean Institute of Electromagnetic Engineering and Science and a member of the Institute of Electrical, Information and Communication Engineers.



Kang-Yoon Lee (SM'12) received the B.S., M.S., and Ph.D. degrees in electrical engineering from Seoul National University, Seoul, South Korea, in 1996, 1998, and 2003, respectively.

From 2003 to 2005, he was with GCT Semiconductor Inc., San Jose, CA, USA, where he was a Manager of the Analog Division and worked on the design of CMOS frequency synthesizer for CDMA/PCS/PDC and single-chip CMOS radio frequency (RF) chip sets for W-CDMA, WLAN, and PHS. From 2005 to 2011, he was with the Department of Electronics Engineering, Konkuk University, as an Associate Professor. Since 2012, he has been with the College of Information and Communication Engineering, Sungkyunkwan University, Suwon, South Korea, where he is currently an Associate Professor. His research interests include implementation of power integrated circuits, CMOS RF transceiver, analog integrated circuits, and analog/digital mixed-mode very large scale integration system design.